Analytica Chimica Acta 1236 (2022) 340574

Contents lists available at ScienceDirect

Analytica Chimica Acta

journal homepage: www.elsevier.com/locate/aca

Serum-based surface-enhanced Raman spectroscopy combined with PCA-RCKNCN for rapid and accurate identification of lung cancer

Dawei Cao [a], Hechuan Lin [a], Ziyang Liu [a], Yuexing Gu [b], Weiwei Hua [b], Xiaowei Cao [b,***], Yayun Qian [b,**], Huiying Xu [a,*], Xinzhong Zhu [a]

[a] College of Mathematics and Computer Science, Zhejiang Normal University, Jinhua, 321004, China
[b] Institute of Translational Medicine, Medical College, Yangzhou University, Yangzhou, 225001, China

HIGHLIGHTS

- A rapid, sensitive, label-free, high-throughput SERS microarray chip was developed.
- Combining SERS with PCA-RCKNCN successfully differentiated the SERS spectra.
- The most prominent spectral features of SERS spectra in PCs loading were captured.
- PCA-RCKNCN was superior to traditional multivariate algorithm in accuracy.

GRAPHICAL ABSTRACT

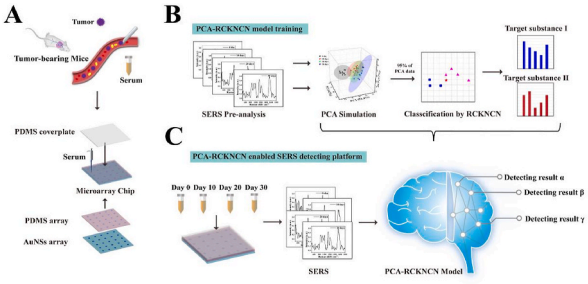

ARTICLE INFO

Keywords:
Surface-enhanced Raman scattering
Lung cancer
Au nanostars
Principal component analysis
Representation coefficient-based k-nearest centroid neighbor

ABSTRACT

Early and precise diagnosis of lung cancer is critical for a better prognosis. However, it is still a challenge to develop an effective strategy for early precisely diagnose and effective treatments. Here, we designed a label-free and highly accurate classification serum analytical platform for identifying mice with lung cancer. Specifically, the microarray chip integrated with Au nanostars (AuNSs) array was employed to measure the surface-enhanced Raman scattering (SERS) spectra of serum of tumor-bearing mice at different stages, and then a recognition model of SERS spectra was constructed using the principal component analysis (PCA)-representation coefficient-based k-nearest centroid neighbor (RCKNCN) algorithm. The microarray chip can realize rapid, sensitive, and high-throughput detection of SERS spectra of serum. RCKNCN based on the PCA-generated features successfully differentiated the SERS spectra of serum of tumor-bearing mice at different stages with a classification accuracy of 100%. The most prominent spectral features for distinguishing different stages were captured in PCs loading plots. This work not only provides a practical SERS chip for the application of SERS technology in cancer screening, but also provides a new idea for analyzing the feature of serum at the spectral level.

* Corresponding author.
** Corresponding author.
*** Corresponding author.
E-mail addresses: cxw19861121@163.com (X. Cao), yyqian@yzu.edu.cn (Y. Qian), xhy@zjnu.edu.cn (H. Xu).

https://doi.org/10.1016/j.aca.2022.340574
Received 27 August 2022; Received in revised form 15 October 2022; Accepted 29 October 2022
Available online 3 November 2022

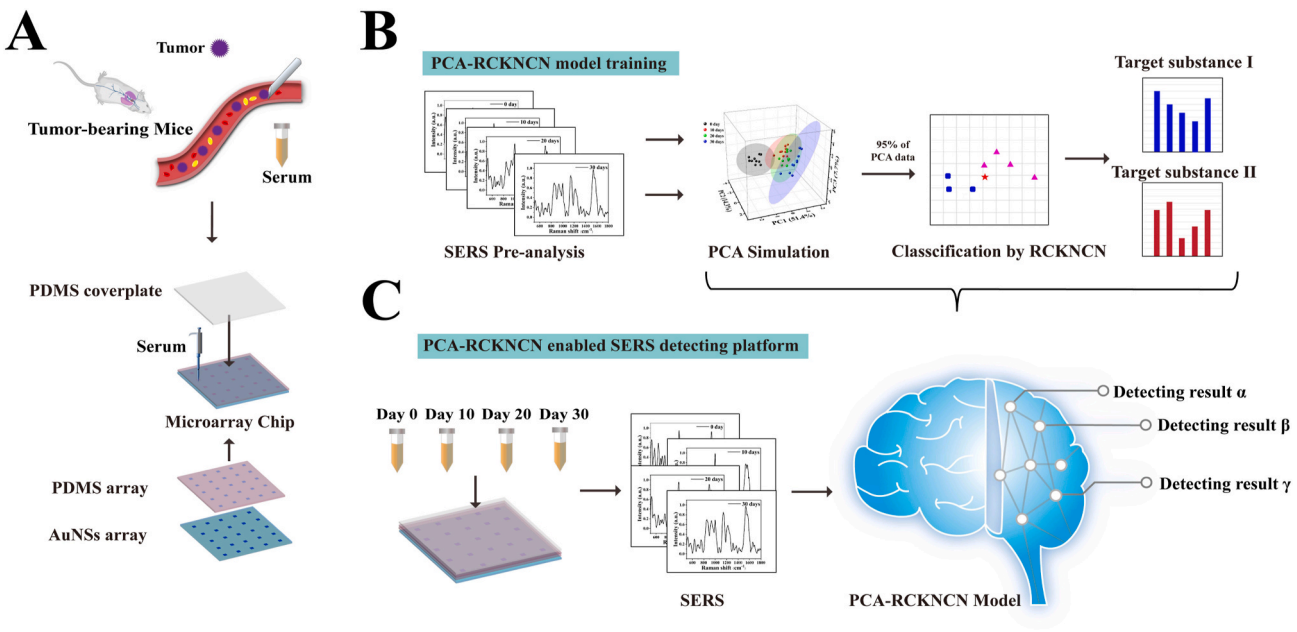

Scheme 1. Schematic representation of label-free detection and identification of tumor-bearing mice at different stages through a combination of SERS and PCA-RCKNCN model. (A) Acquisition of SERS spectra of serum of tumor-bearing mice at different stages. (B) PCA-RCKNCN model training and (C) Analysis of SERS spectra of serum by PCA-RCKNCN model.

1. Introduction

Lung cancer, the most common type of cancer worldwide, accounts for the most significant number of incidences and deaths from malignant tumors [1,2]. Based on histological staging, lung cancer can be divided into small cell lung cancer (SCLC) and non-small cell lung cancer (NSCLC). Of these, NSCLC accounts for over 80% of all lung cancer cases. As lung cancer has a poor prognosis, most lung cancer tumors are identified at a late stage, resulting in low survival rates for all patients [3–5]. The importance of early detection of lung cancer is therefore becoming increasingly apparent [6]. Early diagnosis allows for the rapid distinction of the stage of lung cancer so that appropriate treatment can be administered, thus effectively reducing mortality. Traditional serum tumor marker assays and instrumental tests such as positron emission tomography (PET) have been used for the early diagnosis of lung cancer. However, high positive rate and low sensitivity limits their actual applications. In many cases, these deficiencies make them inaccurate for detection [7,8]. As a disease detection method with great potential, liquid biopsy has been widely used. The serum is one of the most common body fluids and contains rich disease-related information. During the process of cell carcinogenesis, it is often accompanied by changes in the content of substances in serum [9–11]. Through the analysis of serum components, an early diagnosis of cancer can be made. However, current clinical analysis methods cannot provide precise and rapid results. Therefore, a rapid, accurate, and sensitive diagnostic tool is urgently needed for the early diagnosis of lung cancer.

Raman spectroscopy (RS) is an optical analysis method that utilizes the Raman scattering effect for spectral analysis. However, the low Raman signal strength hinders its practical application, that is, the problem of small Raman cross sections during Raman scattering [12–14]. The difference between surface-enhanced Raman spectroscopy (SERS) and Raman spectroscopy is that SERS can increase the detected signal intensity by 10^3–10^8 times with the help of different shapes of noble metal nanomaterials, even reaching the detection level of single molecules [15,16]. This is mainly caused by the enhancement of the electromagnetic (EM) field by the localized surface plasmon resonance effect (LSPR) resulting from the interaction of the incident light with the surface of the nanomaterial [17–21]. SERS has narrow spectral lines, is not susceptible to sudden extinction, and is impervious to water interference [21–23]. At the same time, the uniqueness of the vibrational spectra of molecular features makes them the most suitable for identifying molecules, the "fingerprint" information of a substance [24]. Through "fingerprint" information, the composition and content of substances can be quickly obtained. The early stages of non-small cell lung cancer are undiagnosed due to the lack of obvious symptoms, but the "fingerprint" information from the SERS spectra of serum can be used to identify cellular carcinogenesis based on spectral differences, thus providing a basis for the diagnosis of lung cancer. Therefore, SERS is well suited for the detection and analysis of serum and can be a promising tool for the early diagnosis of lung cancer. Au nanostars (AuNSs) are star-shaped branching nanocrystals with unique optical properties compared to spherical and rod-shaped gold nanoparticles. The tip structure of AuNSs makes them plasma-excited nanomaterial with a large number of "hot spots" [25–27]. At the same time, the optical properties of AuNSs allow them to be used for photothermal and biological imaging, which is promising for disease diagnosis and treatment.

Label-free detection is an unmarked or unmodified method that relies primarily on the analysis and summarization of data. Compared to marker detection, label-free detection has the advantage of being simple, reliable, and inexpensive [28,29]. At present, SERS combined with label-free strategies to detect serum has made some progress [30,31]. However, traditional spectral recognition is mostly manual, requires specialist knowledge, and is inefficient. At the same time, small differences in the Raman spectra of similar substances and errors between the standard and actual spectra often occur during actual testing. In addition, the serum is highly sensitive in its natural environment, which affects the characteristic peaks of the serum components corresponding to the Raman spectra [32]. The use of microarray-based chips for hermetic detection can effectively avoid the problem of contamination caused by the environment [33,32]. At the same time, the extremely complex composition of serum samples has prevented SERS from quickly detecting changes in substances associated with cancer. To overcome the complexity of spectra, many machine learning methods have been used for the automatic identification of spectra. Machine learning is a method of data analysis by extracting features from raw data and making decisions [34,35]. The main ones include principal

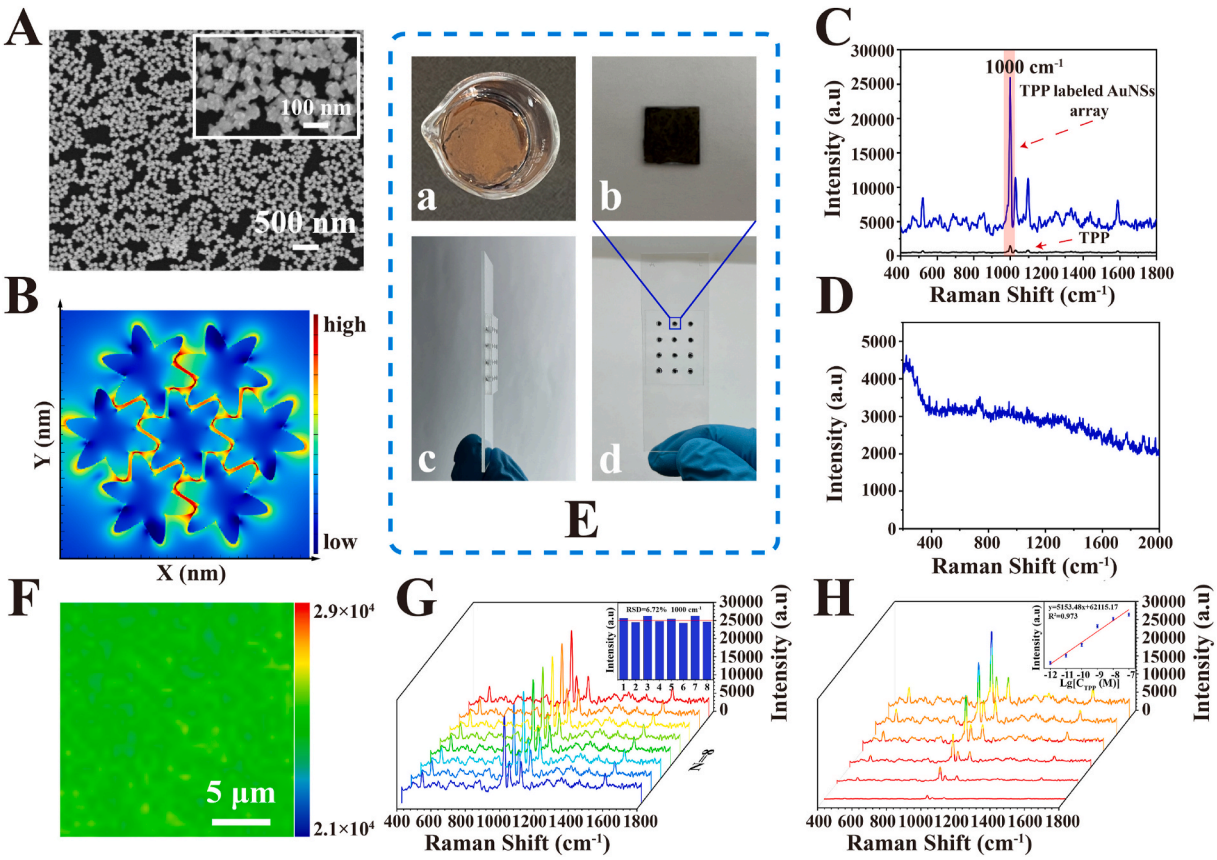

Fig. 1. (A) SEM images of low magnification and high magnification AuNSs array. (B) Images of the electromagnetic field intensity distribution of simulated substrates for AuNSs array. (C) Raman spectra of pure TPP and TPP labeled AuNSs array. (D) SERS spectra of AuNSs array substrates after treatment with 0.1 M KI. (E) Physical photographs of the microarray chip preparation process: (a) Photograph of the self-assembly of the AuNSs array, (b) Glass sheet covering the AuNSs array, (c) and (d) Side and top views of the microarray chip. (F) SERS mapping of the TPP labeled AuNSs array. (G) SERS spectra of 8 different points of AuNSs array labeled with TPP, and the bar chart of the signal intensities at 1000 cm^{-1}. (H) SERS spectra of different concentrations (10^{-7} M, 10^{-8} M, 10^{-9} M, 10^{-10} M, 10^{-11} M, and 10^{-12} M) of TPP were detected using the prepared AuNSs array, and the fitted curves of the logarithm of TPP concentration versus intensity of the characteristic peaks.

component analysis (PCA), support vector machines (SVM), and K-Nearest Neighbor (KNN). These methods are now widely used in applications such as food safety testing, environmental testing, and detection of disease markers [36,37]. However, these algorithms are still unable to quickly and accurately classify biological samples with complex compositions [38,39]. Therefore, an algorithm with better classification performance is needed.

In this work, we proposed a simple and accurate serum detection method for lung cancer diagnosis by combining SERS and PCA-RCKNCN (Scheme 1). The workflow is primarily composed of the following steps: First, AuNSs were synthesized by seed growth method, and then the clean AuNSs arrays obtained by liquid-liquid interface self-assembly method and KI cleaning were used to construct microarray chips. The existence of the AuNSs array and PDMS covering layer enables the microarray chip to be detected under pollution-free conditions with good sensitivity and portability. At the same time, a lung cancer transplantation tumor model was established by subcutaneous injection of human lung cancer A549 cells in mice, and the SERS spectra of the serum of tumor-bearing mice at different stages were obtained. The data set was visualized and features were extracted by noise reduction, smoothing, and normalization of the SERS spectra and the application of the PCA-RCKNCN algorithm. Finally, the PCA-RCKNCN was used to construct SERS spectral identification model for different stages and compared with the conventional PCA-KNN and KNN. It is found that the tumor-bearing mice at different stages can be well distinguished by PCA-RCKNCN, and the accuracy can reach 100%. Overall, this method can be used for the rapid and accurate identification of lung cancer and has a high potential for the diagnosis of lung cancer in the future.

2. Results and discussion

2.1. Characterization of microarray chip

The seed growth method was employed to synthesize AuNSs. Fig. S1 showed that the AuNSs were uniform in size and had good SERS enhancement. The AuNSs were formed by self-assembly at the liquid-liquid interface to form gold films, and it can be seen that the monolayers showed a uniform golden color (Fig. 1E (a)). The AuNSs array was obtained by fishing up the monolayer gold film using a hydrophilic treated glass sheet (Fig. 1E (b)). The prepared AuNSs array was also used to construct microarray chips (Fig. 1E (c and d)). The SEM image of the AuNSs array was shown in Fig. 1A, where the aggregated AuNSs were uniformly distributed on the glass sheet.

After the construction of the microarray chip, finite-difference time-domain (FDTD) simulations were used to investigate the enhancement mechanism of the AuNSs array (Fig. 1B). It can be seen that the "hot spots" were mainly generated adjacent to the sharp spine-like structures of the AuNSs, providing significant SERS enhancement. Meanwhile, the Raman signal enhancement effect was further investigated using TPP (1×10^{-2} M) and TPP (1×10^{-9} M) labeled AuNSs array (Fig. 1C). The Raman enhancement effect of the AuNSs array can be calculated as 2.61×10^{8} by the equation $EF = (I_{SERS}/C_{SERS})/(I_{Raman}/C_{Raman})$. To avoid the residual reductant and active agent on the array surface affecting the SERS detection, a KI of 0.1 M was used to treat the AuNSs array and

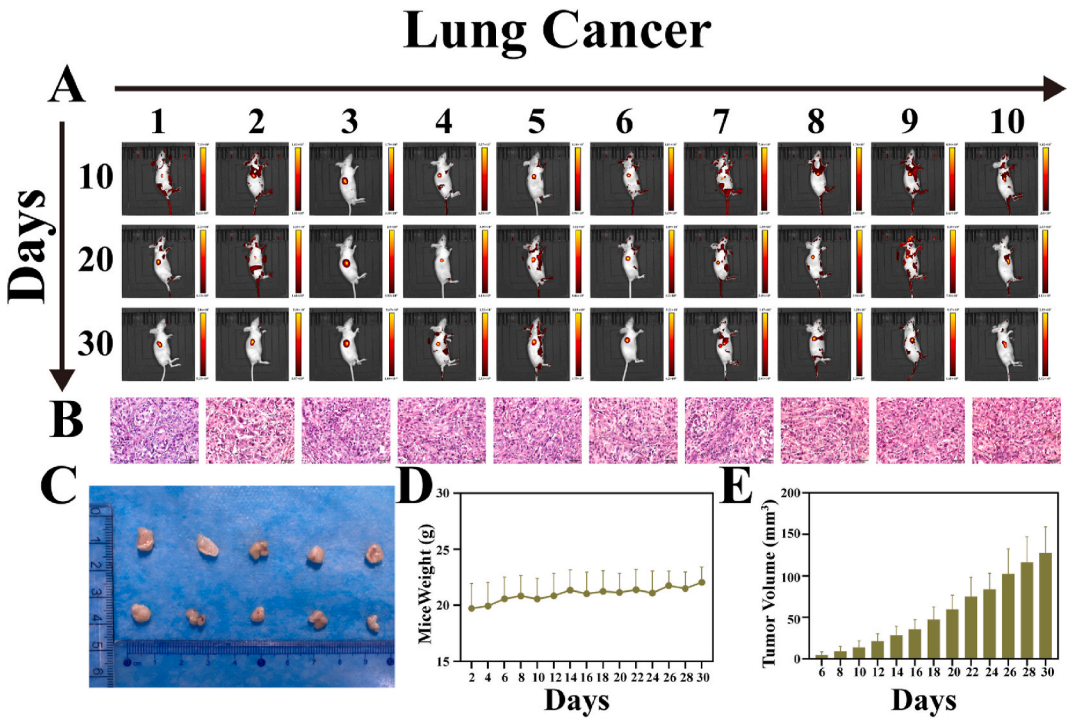

Fig. 2. The nude mice model of lung cancer. (A) The growth of mice and xenograft tumors was recorded every ten days with the live animal imaging system. (B) Transplant tumors were embedded in paraffin and continuously sectioned followed by hematoxylin and eosin (H&E) staining. (C) The lung cancer transplant tumors. (D) The body weights of nude mice bearing A-549 cells. (E) The volume of lung cancer.

obtain pure SERS spectra [40]. The KI replaced impurities on the surface of the AuNSs array via Au–I bonding thus reducing the effect of the signal carried by the substrate itself on the detection (Fig. 1D). In addition, the homogeneity of the AuNSs array was evaluated using TPP (1×10^{-9} M) labeled. Where the variation in signal intensity was represented by red, yellow, blue, and green respectively, Fig. 1F showed a uniform green color overall, although there was some yellow. This indicated that the AuNSs array had good signal uniformity. To evaluate the homogeneity of the AuNSs array substrates, the SERS spectra obtained from eight points scans were selected. As shown in Fig. 1G, the intensity of their SERS spectra varied but the waveforms were broadly consistent. Meanwhile, the relative standard deviation (RSD) of the characteristic peaks corresponding to 1000 cm^{-1} was 6.72%. The sensitivity of the substrate also affects SERS detection. The AuNSs array was used to detect different concentrations of TPP and thus assess its sensitivity. The fitted curve corresponding to the characteristic peak at 1000 cm^{-1} versus the logarithm of the TPP concentration was $y = 5153.48x + 62115.17$ with a relative coefficient (R^2) of 0.973, giving a calculated detection limit of 37.4 fM. The clean microarray chip exhibited good SERS enhancement, homogeneity, and sensitivity and can be used for the detection of tumor-bearing mice serum in the following experiments.

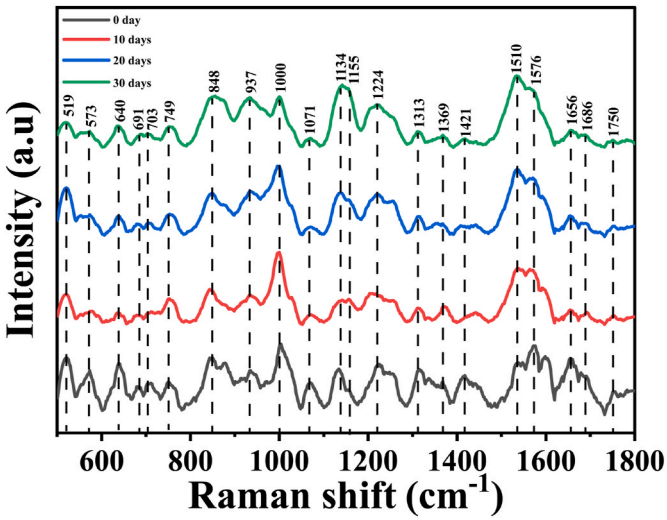

Fig. 3. The mean normalized SERS spectra of tumor-bearing mice serum at different stages (0 day, 10 days, 20 days, 30 days).

2.2. *In vivo tumor establishment*

A transplanted tumor model for lung cancer was established by subcutaneous injection of human lung cancer A549 cells into nude mice. Approximately six days after the injection, the subcutaneous tumors were accessible. The growth of mice and xenograft tumors were recorded on days 10, 20, and 30 with the live animal imaging system (Fig. 2A). Changes in mice body weight (Fig. 2D) and xenograft tumor volume growth (Fig. 2E) were monitored every two days. The whole transplant tumor experiment lasted for 30 days. On day 30, the lung cancer xenograft tumors were collected (Fig. 2C) and embedded in paraffin. After hematoxylin and eosin (H&E) staining, the tumor cell morphology was visualized under a microscope (Fig. 2B). It can be seen that the cells are disordered, large, and dark-stained, all showing the characteristics of the tumor cells. These results confirm that a nude mice model of lung cancer has been successfully established.

2.3. *Comparison of serum SERS spectra of tumor-bearing mice at different stages*

The tumor-bearing mice serum was added dropwise to the prepared microarray chip and then detected using a confocal Raman spectroscopy. The obtained SERS spectra were noise reduced and smoothed to get SERS spectra of tumor-bearing mice serum at different stages (day 0,

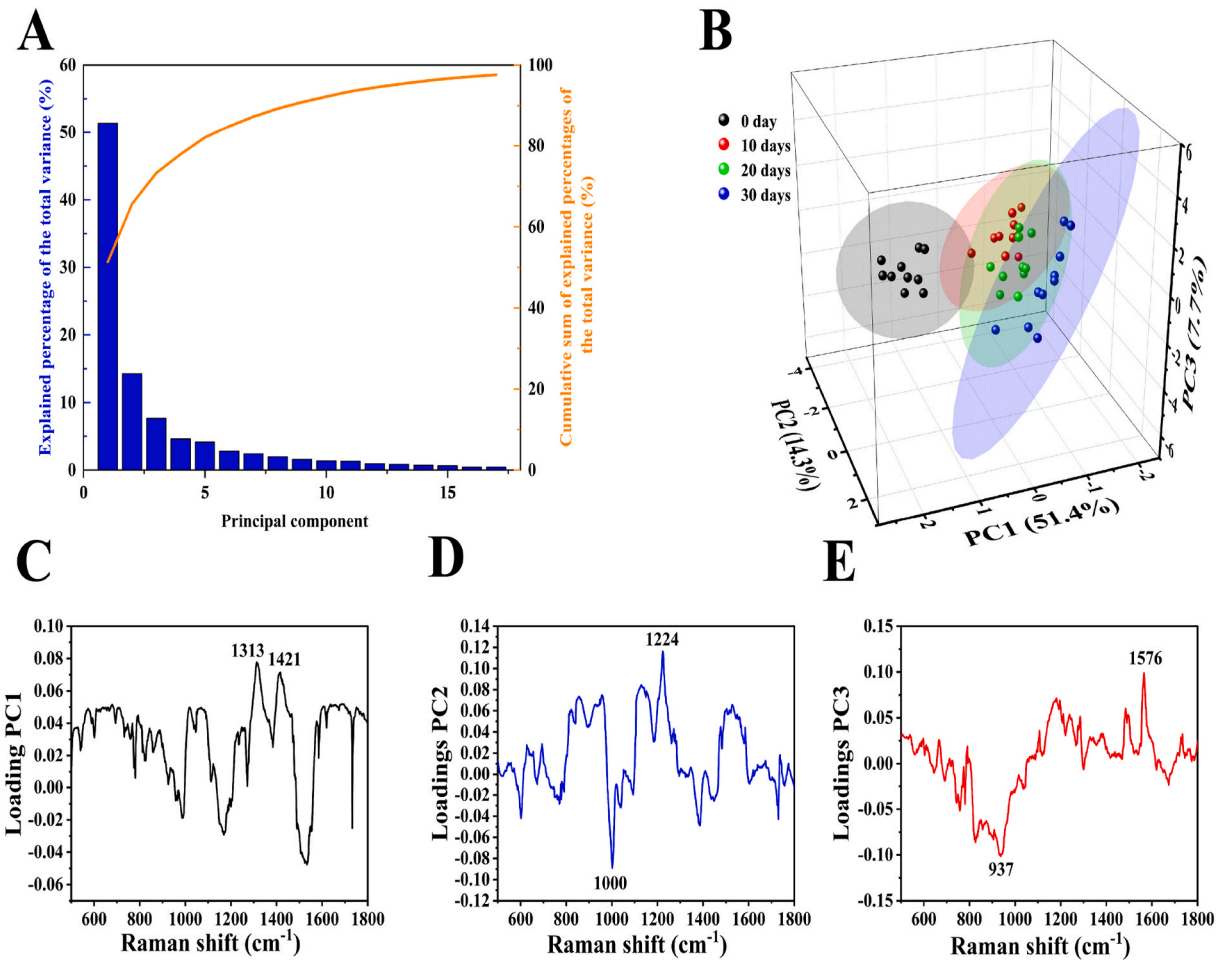

Fig. 4. (A) Scree plot of the variation of component number with the calculated eigenvalues for SERS spectra of the serum. (B) The PCA score plot for the SERS spectra of the tumor-bearing mice serum at different stages. (C) Loadings plot of PC1. (D) Loadings plot of PC2. (E) Loadings plot of PC3.

10, 20, 30) (Figs. S2–S5, Supporting Information). Serum SERS spectra of ten tumor-bearing mice were normalized and used to compare the differences among four stages (Fig. 3). The SERS spectral waveforms of the serum from the different stages of the tumor-bearing mice were essentially the same, except that the intensity of certain characteristic peaks changes. The characteristic peaks were marked by dashed lines, and their assignments are shown in Table S1.

As shown in Fig. 3, the relative intensities of the characteristic peaks tend to decrease during tumor growth at 573 cm^{-1}, 691 cm^{-1}, 703 cm^{-1}, 1000 cm^{-1}, 1071 cm^{-1}, 1313 cm^{-1}, 1224 cm^{-1}, 1576 cm^{-1}, 1656 cm^{-1} and 1686 cm^{-1}. The relative intensity of the peaks tends to increase at 848 cm^{-1}, 937 cm^{-1}, 1134 cm^{-1}, 1155 cm^{-1}, and 1510 cm^{-1}. Meanwhile, it was observed that the intensities of the characteristic peaks at 519 cm^{-1}, 640 cm^{-1}, 1369 cm^{-1}, 1421 cm^{-1}, 1686 cm^{-1}, and 1750 cm^{-1} were changed irregularly in the development of lung cancer. The increase or decrease of the above characteristic peaks reflects the changes in the relative concentrations of biochemical components in serum, which are closely related to the tumor progression stages. For example, the intensity of the characteristic peak at 1313 cm^{-1} attributed to the distorted mode of CH_3CH_2 collagen decreases progressively with tumor growth [41,42]. This may be due to the increased concentration of metalloproteinases during tumor growth, leading to the cleavage of large amounts of collagen, thereby reducing the overall level of collagen in the serum. At the same time, the Raman peaks of tryptophan/cytosine, guanine (573 cm^{-1}), methionine (691 cm^{-1}), phenylalanine (1000 cm^{-1}), and lipids (703 cm^{-1}, 1071 cm^{-1} and 1656 cm^{-1}) decreased [43,44]. There were significant increases in the Raman peaks for glucose (848 cm^{-1}), proteins, carbohydrates (937 cm^{-1}), fatty acids (1134 cm^{-1}), carotenoids (1155 cm^{-1}), and ring breathing modes in the DNA bases (1510 cm^{-1}), which may be associated with abnormal tumor metabolism [41,42,45]. At an overall level, with the development of lung cancer, the expression levels of protein, carotenoid, sugar, and nucleic acid in the serum of tumor-bearing mice gradually increased. The fingerprint features of SERS spectra are of great clinical significance for the diagnosis of lung cancer. In conclusion, we initially explored differences in SERS profiles of serum from tumor-bearing mice at different stages.

2.4. Multivariate analysis

To further differentiate the SERS spectra at different stages, PCA-RCKNCN was applied to analyze the SERS spectra and establish a SERS spectra identification model. PCA is a statistical technique for simplifying complex data sets and determining the key variables in a multidimensional data set that best explain the differences in the observations [46]. Here, most of the important information was distributed over the first few PCs and the contributions of the rest of the PCs are negligible. Fig. 4A showed the contribution of eigenvalues of each PC to the total variance of all SERS spectra. It was observed that the eigenvalues reduced rapidly with increasing PC numbers and only the first few PCs hold the maximum variance of the obtained SERS spectra data. PC1 is the largest eigenvector, which shows the direction of the largest difference between SERS spectra. PC2 is the second largest eigenvector, which is orthogonal to PC1 [47]. It can be seen that the first thirteen

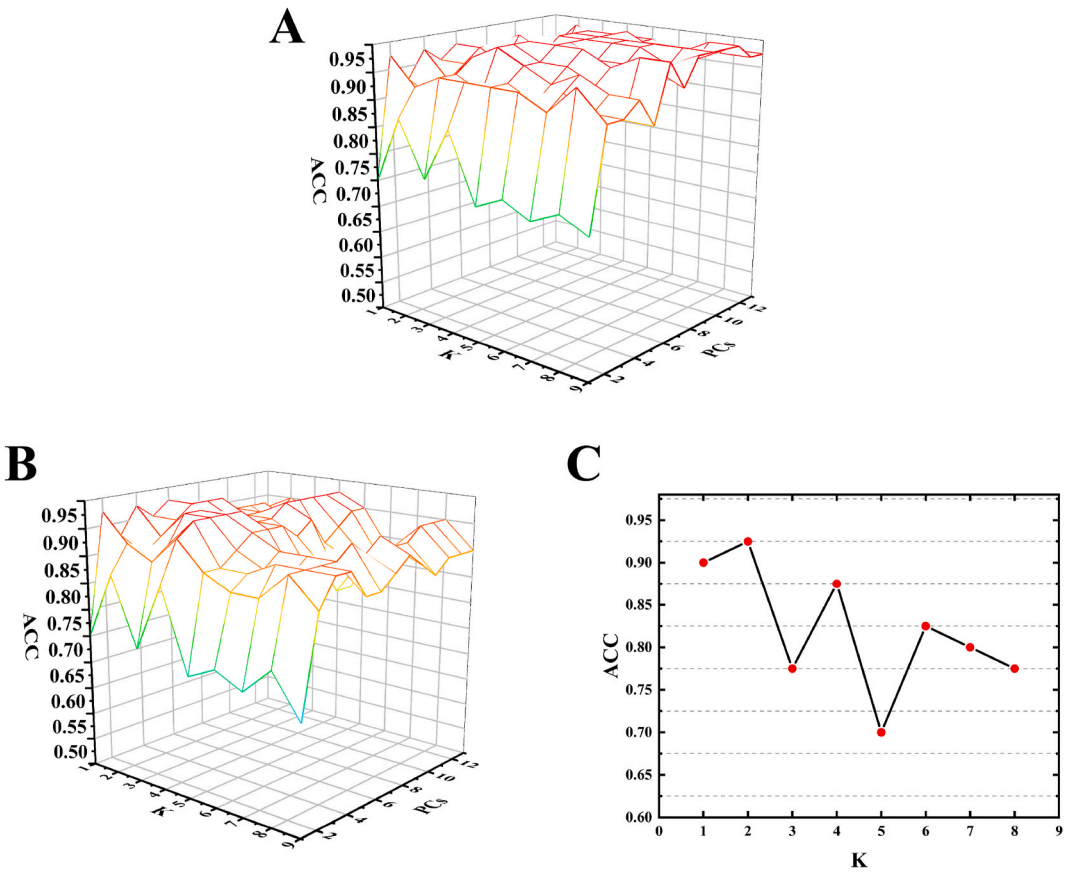

Fig. 5. (A) The accuracy of PCA-RCKNCN under different PCs and different K values. (B) The accuracy of PCA-KNN under different PCs and different K values. (C) The accuracy of KNN under different K values.

principal components described more than 95% of the variation of all SERS spectra. The score plot reflected the similarities and differences among the SERS spectra of tumor-bearing mice serum at different stages (Fig. 4B). The contribution rates of PC1, PC2, and PC3 were 51.4%, 14.3%, and 7.7%, respectively, with a total of 73.4%, indicating that PC1, PC2, and PC3 had reflected most information of the original spectra data. Most of the projection points in each stage can be surrounded by an obvious 95% confidence ellipsoid. Each dot in the plot represented one SERS spectrum with dimension reduction. The four separate groups clearly show the separation of SERS spectra at different stages. SERS spectra of 0 day and 30 days were distinguishable and they were well divided into two distinct groups. This was mainly attributed to the difference in biochemical composition in serum. On the 10 days of tumor growth, 10 days groups were adjacent to 0 day groups. When the tumor-bearing mice were raised for 20 days, their groups were far away from the 0 day groups and partially overlapped with 10 days groups and 30 days groups.

The obvious characteristic peaks were obtained from PC1, PC2, and PC3 loading plots to determine the critical spectral features of different stages. Load values of PC1, PC2, and PC3 were shown in Fig. 4C, D, and 4E. The greater the absolute value of load value, the greater the contribution rate to the principal components and the greater the influence on discrimination between the SERS spectra at different stages. According to the load value of PC1 with a contribution rate of 51.4%, the positive peaks at 1313 cm^{-1} (CH_3CH_2 twisting mode of collagen), 1421 cm^{-1} (Deoxyribose, (B, Z-marker)) explained the high load value of PC1 (Fig. 4C). PC1 reflected the importance of high levels of nucleic acid, collagen, which contributed most to distinguishing the SERS spectra at a different stage. In addition, the PC2 and PC3 high load values were mainly explained by the positive peaks at 1224 cm^{-1} (Amide III (β sheet structure)), 1576 cm^{-1} (Guanine (N_3)) and the negative peaks at 937 cm^{-1} (Proline, hydroxyproline, (C–C) skeletal of collagen backbone), 1000 cm^{-1} (Phenylalanine Bound & free NADH). It was worth noting that although it explained only 14.3% and 7.7% of the variance, PC2 and PC3 directly reflected the importance of high levels of some amino acids in PCA analysis (Fig. 4D and E). In particular, the obvious characteristic peaks from the PC1, PC2, and PC3 loading plots can be well classified (Fig. S6, Supporting Information).

After PCA processing, we selected the first thirteen PCs which accounted for 95% of the total variance were used as features for PCA-RCKNCN. RCKNCN was a novel representation coefficient-based k-nearest centroid neighbor classification method. The classification principle of RCKNCN was shown in Fig. S7 (Supporting Information). It considered the ideas of nearest centroid neighborhood (NCN) and the linear representation of the neighbors and learned to weigh the neighbors adaptively [48]. In order to analyze the performance of the PCA-RCKNCN model, this model was compared with the traditional PCA-KNN and KNN. Through Leave-One-Out Cross Validation (LOOCV), the accuracy of PCA-RCKNCN and PCA-KNN based on different PCs and K values were obtained, as shown in Fig. 5A and B. It was clear that the overall accuracy of PCA-RCKNCN was higher than PCA-KNN and was not sensitive to the selection of K value. When the K and PCs values were 4 and 6, the discrimination accuracy was the highest. When using KNN, it can be seen that the maximum discrimination accuracy was obtained when the K value was 2, as shown in Fig. 5C.

These values were put into PCA-RCKNCN, PCA-KNN, and KNN to calculate the confusion matrix, respectively (Fig. S8, Supporting Information). This result demonstrated a good recognition ability of PCA-RCKNCN on the SERS spectra at 0 day, 10 days, 20 days, and 30 days groups. Compared with PCA-KNN and KNN, PCA-RCKNCN had significant advantages in the analysis of SERS spectral data. Therefore, PCA-RCKNCN was employed as the statistical tool to accurately distinguish

the tumor-bearing mice at different stages based on the specific spectral features of serum.

3. Conclusions

In summary, we have successfully demonstrated the diagnosis of the SERS spectra of serum from tumor-bearing mice subcutaneously injected with human lung cancer A549 cells using SERS technology and PCA-RCKNCN. A novel microfluidic SERS chip integrated with AuNSs array was proposed, which exhibited good uniformity, high sensitivity, excellent SERS enhancement effect, and portability. Using the designed microfluidic chip, the high-quality SERS signals of serum of tumor-bearing mice at different stages can be acquired and a series of characteristic peaks representative of various biomolecules have been detected. The PCA-RCKNCN model successfully differentiated the SERS spectra of serum of tumor-bearing mice at different stages. The most prominent spectral features of SERS spectra in PCs loading suggested interesting the serum from tumor-bearing mice specific biomolecular differences, including an obvious change in the relative amounts of nucleic acid, collagen, and some amino acids. Compared with the traditional PCA-KNN and KNN, the PCA-RCKNCN model based on principal component variables had better accuracy for spectral classification. The results from this exploratory study demonstrated tremendous promise for the development of a serum analytical platform by combining SERS and PCA-RCKNCN for non-invasive detection and screening of lung cancer. Our next step will be to conduct more detailed prospective studies to verify the reliability of this new lung cancer detection method.

CRediT authorship contribution statement

Dawei Cao: Methodology, Validation, Formal analysis, Investigation, Data curation, Writing – original draft. **Hechuan Lin:** Investigation, Resources, Data curation. **Ziyang Liu:** Methodology, Software, Validation. **Yuexing Gu:** Formal analysis, Investigation, Data curation. **Weiwei Hua:** Methodology, Resources, Validation. **Xiaowei Cao:** Writing – review & editing, Project administration, Funding acquisition. **Yayun Qian:** Writing – review & editing, Supervision, Project administration. **Huiying Xu:** Writing – review & editing, Visualization, Supervision, Project administration, Funding acquisition. **Xinzhong Zhu:** Writing – review & editing, Visualization, Supervision, Project administration, Funding acquisition.

Declaration of competing interest

The authors declare that they have no known competing financial interests or personal relationships that could have appeared to influence the work reported in this paper.

Data availability

Data will be made available on request.

Acknowledgments

This work was supported by the Natural Science Foundation of China (project no. 61976196), Outstanding Talents of “Ten Thousand Talents Plan” in Zhejiang Province (project no. 2018R51001), Zhejiang Provincial Natural Science Foundation of China (project no. LZ22F030003), the Social Development Foundation of Jiangsu (No. BE2018684), the Major Programs of Natural Science Foundation of Higher Education in Jiangsu Province (19KJA480003) and the Administration of Traditional Chinese Medicine Project of Jiangsu Province (MS2021081).

Appendix A. Supplementary data

Supplementary data to this article can be found online at https://doi.org/10.1016/j.aca.2022.340574.

References

[1] A. Khanmohammadi, A. Aghaie, E. Vahedi, A. Qazvini, M. Ghanei, A. Afkhami, A. Hajian, H. Bagheri, Talanta 206 (2020), 120251.
[2] X. Liu, M. Ma, X. Duan, H. Zhang, M. Yang, Clin. Transl. Oncol. 19 (2017) 587–592.
[3] T. Luo, L. Yan, H. Liu, J. Buon, Clin. Transl. Oncol. 25 (2020) 1517–1524.
[4] L. Zhou, C. Xing, D. Zhou, R. Yang, M. Cai, Open Med. 15 (2020) 986–996.
[5] F. Xu, P. Xu, W. Cui, W. Gong, Y. Wei, B. Liu, J. Dong, Oncol. Lett. 16 (2018) 483–490.
[6] M. Feng, X. Ye, B. Chen, J. Zhang, M. Lin, H. Zhou, M. Huang, Y. Chen, Y. Zhu, B. Xiao, C. Huang, R.L. Katz, C. Bai, J. Cancer Res. Clin. Oncol. 17 (2020) 2397–2405.
[7] W.-R. Liu, B. Zhang, C. Chen, Y. Li, X. Ye, D.-J. Tang, J.-C. Zhang, J. Ma, Y.-L. Zhou, X.-J. Fan, D.-S. Yue, C.-G. Li, H. Zhang, Y.-C. Ma, Y.-S. Huo, Z.-F. Zhang, S.-Y. He, C.-L. Wang, Thorac. Cancer 11 (2020) 3234–3242.
[8] J. Marrugo-Ramirez, M. Mir, J. Samitier, Int. J. Mol. Sci. 19 (2018) 2877.
[9] C. Rolfo, P.C. Mack, G.V. Scagliotti, P. Baas, F. Barlesi, T.G. Bivona, R.S. Herbst, T. S. Mok, N. Peled, R. Pirker, L.E. Raez, M. Reck, J.W. Riess, L.V. Sequist, F. A. Shepherd, L.M. Sholl, D.S.W. Tan, H.A. Wakelee, I.I. Wistuba, M.W. Wynes, D. P. Carbone, F.R. Hirsch, D.R. Gandara, J. Thorac. Oncol. 13 (2018) 1248–1268.
[10] W. Yu, J. Hurley, D. Roberts, S.K. Chakrabortty, D. Enderle, M. Noerholm, X. O. Breakefield, J.K. Skog, Ann. Oncol. 32 (2021) 466–477.
[11] R.R. Jones, D.C. Hooper, L. Zhang, D. Wolverson, V.K. Valev, Nanoscale Res. Lett. 14 (2019) 231.
[12] K. Xu, R. Zhou, K. Takei, M. Hong, Adv. Sci. 6 (2019), 1900925.
[13] X. Xi, C. Liang, Front. Chem. 9 (2021), 665841.
[14] S.-Y. Ding, J. Yi, J.-F. Li, B. Ren, D.-Y. Wu, R. Panneerselvam, Z.-Q. Tian, Nat. Rev. Mater. 1 (2016), 16021.
[15] Q.Q. Fu, H.W.L. Liu, Z. Wu, A. Liu, C.Z. Yao, X.Q. Li, W. Xiao, S.T. Yu, Z. Luo, Y. Tang, J. Nanobiotechnol. 13 (2015) 81.
[16] Y.D. Sun, L. Fang, Y. Yi, A.B. Feng, K. Zhang, J.J. Xu, J. Nanobiotechnol. 20 (2022) 285.
[17] X. Wang, S.-C. Huang, S. Hu, S. Yan, B. Ren, Nat. Rev. Phys. 2 (2020) 253–271.
[18] A.B. Zrimsek, N. Chiang, M. Mattei, S. Zaleski, M.O. McAnally, C.T. Chapman, A.-I. Henry, G.C. Schatz, R.P. Van Duyne, Chem. Rev. 117 (2017) 7583–7613.
[19] A.S.D.S. Indrasekara, J. Appl. Phys. 129 (2021), 231102.
[20] J. Kim, K. Sim, S. Cha, J.-W. Oh, J.-M. Nam, J. Raman Spectrosc. 52 (2021) 375–385.
[21] M. Fan, G.F.S. Andrade, A.G. Brolo, Anal. Chim. Acta 1097 (2020) 1–29.
[22] A.I. Perez-Jimenez, D. Lyu, Z. Lu, G. Liu, B. Ren, Chem. Sci. 11 (2020) 4563–4577.
[23] C. Zong, M. Xu, L.-J. Xu, T. Wei, X. Ma, X.-S. Zheng, R. Hu, B. Ren, Chem. Rev. 118 (2018) 4946–4980.
[24] M. Monsefi, T. Tajerian, A. Rowan, J. Nanostruct. 10 (2020) 198–205.
[25] Y. Tang, A. Kuzume, K. Yamamoto, Chem. Lett. 50 (2021) 248–251.
[26] S. Wang, Y. Zhang, Y. Li, K. Chen, Y. Dai, D. Zhou, A. Ali, S. Yang, X. Xu, T. Jiang, L. Zhu, Mater. Des. 205 (2021), 109707.
[27] S.R. Mahmoodi, P. Xie, M. Allen, M. Javanmard, IEEE Sens. Lett. 4 (2020), 4500104.
[28] Y. Wei, W. Zhou, Y. Wu, H. Zhu, ACS Sens. 6 (2021) 4304–4314.
[29] W. Li, G. Wu, X. Zhang, A. Yue, W. Du, J. Zhao, D. Liu, Chem. J. Chin. Univ. 41 (2020) 872–883.
[30] Z. Wang, S. Wang, G. Chen, X. Su, Sensor. Actuator. B Chem. 347 (2021), 130612.
[31] A.V. Orlov, A.V. Pushkarev, S.L. Znoyko, D.O. Novichikhin, V.A. Bragina, B. G. Gorshkov, P.I. Nikitin, Biosens. Bioelectron. 159 (2020), 112187.
[32] F. Lussier, V. Thibault, B. Charron, G.Q. Wallace, J.-F. Masson, Trac-Trend. Anal. Chem. 124 (2020), 115796.
[33] T. Lin, Y.-L. Song, P. Kuang, S. Chen, Z. Mao, T.-T. Zeng, Nanomedicine 16 (2021) 2389–2406.
[34] S. Park, J. Lee, S. Khan, A. Wahab, M. Kim, Sensors 22 (2022) 596.
[35] A. Barucci, C. D'Andrea, E. Farnesi, M. Banchelli, C. Amicucci, M. de Angelis, B. Hwang, P. Matteini, Analyst 146 (2021) 674–682.
[36] T. Rojalin, D. Antonio, A. Kulkarni, R.P. Carney, Appl. Spectrosc. 76 (2022) 485–495.
[37] M. Wang, X. Cao, W. Lu, L. Tao, H. Zhao, Y. Wang, M. Guo, J. Dong, W. Qian, RSC Adv. 4 (2014) 64225–64234.
[38] Q.B. Li, W.J. Li, J.L. Zhang, Z. Xu, Analyst 143 (2018) 2807–2811.
[39] U. Parlatan, M.T. Inanc, B.Y. Ozgor, E. Oral, E. Bastu, M.B. Unlu, G. Basar, Sci. Rep. 9 (2019), 19795.
[40] N. Stone, C. Kendall, N. Shepherd, P. Crow, H. Barr, J. Raman Spectrosc. 33 (2002) 564–573.
[41] N. Stone, C. Kendall, J. Smith, P. Crow, H. Barr, Faraday Discuss 126 (2004) 141–157.
[42] R.J. Lakshmi, V.B. Kartha, C.M. Krishna, J.G.R. Solomon, G. Ullas, P.U. Devi, Radiat. Res. 157 (2002) 175–182.
[43] G. Shetty, C. Kendall, N. Shepherd, N. Stone, H. Barr, Br. J. Cancer 94 (2006) 1460–1464.
[44] C. Krafft, L. Neudert, T. Simat, R. Salzer, Spectrochim. Acta Mol. Biomol. Spectrosc. 61 (2005) 1529–1535.

[45] S.S. Du, M.K. Su, Y.F. Jiang, F.F. Yu, Y. Xu, X.F. Lou, T. Yu, H.L. Liu, ACS Sens. 4 (2019) 1798–1805.
[46] P. Moitra, A. Chaichi, S.M.A. Hasan, K. Dighe, M. Alafeef, A. Prasad, M.R. Gartia, D. Pan, Biosens. Bioelectron. 208 (2022), 114200.
[47] D. Ishwar, R. Haldavnekar, S. Das, B. Tan, K. Venkatakrishnan, ACS Nano 16 (2022) 10859–10877.
[48] Z.M. Guo, M.M. Wang, A.O. Barimah, Q.S. Chen, H.H. Li, J.Y. Shi, H.R. El-Seedi, X. B. Zou, Int. J. Food Microbiol. 338 (2021), 108990.